Published in final edited form as:
J Immunol. 2011 April 1; 186(7): 4088–4097. doi:10.4049/jimmunol.1001139.

Conformational switching in ezrin regulates morphological and cytoskeletal changes required for B cell chemotaxis

Neetha Parameswaran, **Ken Matsui**, and **Neetu Gupta**
Department of Immunology, Lerner Research Institute, Cleveland Clinic, 9500 Euclid Avenue, NE40, Cleveland, OH 44195

Abstract

B cell chemotaxis occurs in response to specific chemokine gradients and is critical for homeostasis and immune response. The molecular regulation of B cell membrane-actin interactions during migration is poorly understood. In this study we report a role for ezrin, a member of the membrane-cytoskeleton crosslinking Ezrin-Radixin-Moesin (ERM) proteins, in the regulation of the earliest steps of B cell polarization and chemotaxis. We visualized chemokine-induced changes in murine B cell morphology using scanning electron microscopy, and spatiotemporal dynamics of ezrin in B cells using epifluorescence and total internal reflection microscopy. Upon chemokine stimulation ezrin is transiently dephosphorylated to assume an inactive conformation, and localizes to the lamellipodia. B cells expressing a phosphomimetic conformationally active mutant of ezrin, or those in which ezrin dephosphorylation was pharmacologically inhibited displayed impaired microvillar dynamics, morphological polarization and chemotaxis. Our data suggest a two-fold involvement of ezrin in B cell migration whereby it first undergoes chemokine-induced dephosphorylation to facilitate membrane flexibility, followed by relocalization to the actin-rich lamellipodia for dynamic forward protrusion of the cells.

Keywords

B cell; chemotaxis; imaging; ezrin; plasma membrane; actin

INTRODUCTION

B cell homing and recirculation are essential features of B cell immunity. B cells display varied responsiveness to chemokines such as B lymphocyte chemokine (BLC/CXCL13), stromal cell-derived factor 1 alpha (SDF-1α/ CXCL12), and secondary lymphoid organ chemokine (SLC/CCL21) during their lifetime (1). Aberrant expression or signaling mediated by chemokines and their cognate receptors have been implicated in the pathogenesis of B cell disorders such as lupus (2), rheumatoid arthritis (3), leukemias (4, 5) and viral infections (6). Chemotaxis occurs when cells respond to gradients of chemokines displayed on endothelial cells lining the blood vessels, or on stromal cells in secondary lymphoid organs (7). In situ imaging of lymph nodes from immunized mice using two-photon microscopy revealed spontaneously motile B cells that pause temporarily upon antigen binding, followed by preferential migration towards the T cell zone (8). During both forms of motility B cells display a polarized morphology. Cell motility must require

Correspondence to: Neetu Gupta (guptan@ccf.org), Ph: 216-444-7455, FAX: 216-444-9329.

AUTHOR CONTRIBUTIONS N.G. and N.P. designed research; N.P. and K.M. performed research; N.G. and N.P. analyzed data; N.P. contributed new analytical tools; N.G. and N.P. prepared the manuscript.

The online version of this article contains supplemental material.

evolution of membrane-actin contacts at the leading edge that provide the protrusive force for migration (9). In addition, intra- and extravasation of B cells through blood vessels during homing to and from lymphoid organs must involve dynamic cell shape changes involving plasma membrane and cytoskeleton reorganization (10)

The importance of cytoskeletal rearrangement in B cell polarization and migration was demonstrated using mice lacking proteins involved in chemokine receptor signaling. DOCK2-deficient mice exhibit poor B lymphocyte migration and disrupted lymphoid architecture due to impaired activation of the Rho GTPase family member Rac (11). SWAP-70, a Rac-interacting protein involved in actin rearrangement regulates integrin-mediated adhesion of B cells, facilitating B cell entry into lymph nodes (12). The Rap1 and 2 GTPases play an important role in mediating adhesion and cytoskeletal reorganization during SDF-1α-dependent migration as well as marginal zone B cell development (13-16). Integrin-mediated adhesion, B cell migration in response to SDF-1α and BLC, as well as in vivo homing to lymphoid organs, are impaired in mice deficient in Bruton's tyrosine kinase (17). While several studies have underscored the importance of Rho and Rap family GTPases in orchestrating actin rearrangements involved in migration (18-21), the regulation of contact between the plasma membrane and actin filaments at the protruding front is not well understood. The ezrin-radixin-moesin (ERM) family consists of actin-binding proteins that link the plasma membrane to the underlying cortical actin meshwork and thus have the potential to regulate cellular events that require membrane remodeling, including proliferation, morphogenesis, migration, and adhesion (22, 23). ERM proteins can exist in two alternate conformations, a closed conformation in which the N- and C-termini are engaged in an intramolecular association, or an open conformation that results from binding to phosphatidylinositol 4,5 bisphosphate (PIP_2) followed by phosphorylation of a conserved regulatory threonine residue in the C-terminal actin-binding domain (22, 24). The open conformation enables ERM proteins to link the membrane to the cytoskeleton (24). Lymphocyte-oriented kinase (LOK) has been identified as the kinase that phosphorylates ERM proteins in lymphocytes leading to their activation (25). Inhibiting the phosphorylation of ERM proteins by knocking out LOK in mice results in increased F-actin polarization and lymphocyte migration in response to SDF-1α (25). Phospholipase C-mediated hydrolysis of membrane PIP_2 plays an important role in initiating the inactivation of ERM proteins in chemokine-stimulated T cells (26).

We have previously reported that stimulation of the BCR results in dephosphorylation of ezrin at threonine 567 (T567), transiently dissociating it from Csk-binding protein (Cbp/PAG), a transmembrane protein enriched in lipid rafts (27). Ezrin concomitantly dissociates from actin filaments, thus facilitating antigen-induced lipid raft coalescence (27). Thus, conformational changes in ezrin have the potential to regulate membrane-actin contacts when a B cell encounters chemokine gradients. Increased ezrin expression has been correlated with highly metastatic cancers further supporting a role for this protein in migratory behavior of cells (28).

To investigate the participation of ezrin in the earliest morphological changes that precede cell migration we performed high-resolution visual analysis of B cell morphology and ezrin in live resting B cells and those undergoing migration. We show that the regulatory threonine residue in ezrin and moesin is transiently dephosphorylated in response to chemokine stimulation. Preventing dephosphorylation or expressing a phosphomimetic mutant of ezrin inhibits B cell migration. Our data demonstrate that transient dephosphorylation of ezrin regulates membrane flexibility that the B cell must achieve during migration. Furthermore, switching between the tethering and untethering conformations of ezrin may facilitate rapid changes in membrane-actin interaction at the front of migrating B cells.

MATERIALS AND METHODS

Cells, antibodies and other reagents

The murine 2PK3 B lymphoma cell line was cultured in B cell growth medium consisting of DMEM and 10% FBS. Primary B cells were purified from spleens of C57BL/6 mice by negative depletion using CD43 MicroBeads (Miltenyi Biotec). Rabbit polyclonal antibodies to phosphoThrERM, ERK1/2, phosphoERK1/2, JNK, phosphoJNK, Akt and phosphoAkt were from Cell Signaling Technology and antibody to ezrin was from Millipore. HRP-conjugated goat anti-rabbit secondary antibodies and FITC-conjugated antibody to rabbit-IgG were from The Jackson Research Laboratories. Flow cytometry antibodies, including biotin-conjugated CXCR5, FITC-conjugated B220, PE-conjugated CD19, PE-conjugated CD44, allophycocyanin (APC)-conjugated CD45.2 and PE-conjugated streptavidin were from BD-Biosciences. AlexaFluor 594-conjugated antibody to rabbit-IgG, rhodamine-conjugated phalloidin and AlexaFluor 488-conjugated phalloidin were from Invitrogen.

Mice

C57BL/6 and B6.SJL mice were purchased from The Jackson Laboratory, and used at 8-12 wk of age. All experiments involving mice were approved by the Institutional Animal Care and Use Committee of the Cleveland Clinic.

Plasmids and transfection

Ezrin-pIRES2-EGFP was constructed by subcloning full-length ezrin (1-586) into the Xho I and EcoR I sites of pIRES2-EGFP vector (Clonetech). The threonine 567 residue in ezrin was mutated to aspartic acid (T567D) using the QuikChange® II Site-Directed mutagenesis kit (Stratagene). In order to generate YFP fusions of Ezrin, the stop codon TAA in Ezrin-pIRES2-EGFP was mutated to GGA (Glycine), and the stop codon-mutated wild type ezrin was subcloned into the Xho I and EcoR I sites of the vector pEYFP-N1 (Clonetech). The T567 site in the resulting fusion construct (Ez-YFP) was mutated to aspartic acid to generate a T567D-YFP fusion protein (TD-YFP). 2PK3 cells were transfected with 3-6 μg of the appropriate plasmids using Amaxa Nucleofector II (Lonza). Stable transfectants were generated by selecting for G418-resistance and sorting for high GFP expression using the Aria I cell sorter (Becton Dickinson).

Cell lysis and immunoblotting

Purified splenic B cells or 2PK3 cells were stimulated with BLC or SDF-1α (R&D Systems) at 37 °C for the indicated times, lysed in buffer containing 20 mM Tris-Cl, pH 8.3, 150 mM NaCl, 1 mM EDTA, 1% NP-40, and protease and phosphatase inhibitors (5 mg/ml pepstatin A, 1 mM PMSF, 0.5 μM iodoacetamide, 1 mM sodium metavanadate, 10 mM sodium flouride, 25 mM β-glycerophosphate and 1 nM calyculin A) for 30 min on ice, and lysates were subjected to SDS-PAGE followed by probing with appropriate primary and secondary antibodies. In some experiments, prior to stimulation with chemokine the cells were either pretreated for 30 min with the Ser/Thr phosphatase inhibitor calyculin A or pretreated for 10 min with the PLC inhibitor U-73122.

Transwell migration assay

Chemotaxis assays were performed with purified splenic B cells or with transiently transfected 2PK3 cells using uncoated 5-μm transwell filters (Corning Costar) as described (29). Briefly, cells were added to transwell inserts placed in wells containing medium with or without the chemokine, harvested after 4 h and counted by flow cytometry using timed acquisition for 1 min with time resolution set at 10 milliseconds. Data were analyzed with FlowJo software (Treestar).

In vivo B cell homing assay

Five million per ml purified CD45.2$^+$ splenic B cells from C57BL/6 mice were treated with calyculin A or DMSO for 30 min and washed. Ten million cells were injected intravenously into CD45.1$^+$ B6.SJL recipients. Recipients were sacrificed 1.5 h or 26 h later to harvest blood, lymph nodes and spleen. Splenocytes were stained with antibodies to B220 and CD45.2 followed by flow cytometry and data analysis.

Scanning electron microscopy (Scanning EM)

Cells were adhered on to poly L-lysine (PLL)-coated coverslips, and left unstimulated or stimulated with 10 μg/ml BLC, followed by immediate fixing in PFA and glutaraldehyde. Samples were subsequently rinsed, dehydrated with series of graded ethanol, subjected to critical point drying and sputter coated with a thin layer of gold. Processed samples were viewed with a JEOL JSM 5310 Scanning Microscope at 7500X magnification and images were captured using JEOL Orion Image acquisition and handling controls.

Epifluorescence and TIRF microscopy

For ezrin and actin polarization experiments, splenic B cells, 2PK3 B cells, Ez-YFP- or TD-YFP-expressing 2PK3 cells were adhered to PLL or fibronectin-coated coverslips, followed by stimulation with BLC. Cells were fixed immediately with 4% PFA followed by permeabilization and staining with rhodamine-conjugated phalloidin for 1 h at 4 °C. After washing the cells were covered with 200 μl of PBS, and examined by microscopy. For staining endogenous ezrin and moesin fixed cells were blocked with 10 μg of goat IgG for 15 min followed by staining with ezrin or moesin antibody for 2 h at 4 °C, and FITC- or AlexaFluor 594-conjugated rabbit-IgG for 30 min. For staining CD44, 2PK3 B cells transiently transfected with TD-YFP were adhered to PLL-coated coverslips, followed by stimulation with 10 μg/ml of BLC. Cells were fixed immediately with 4% PFA and stained with PE-conjugated antibody to CD44 for 30 min at 4 °C. After washing the cells were covered with 200 μl of PBS, and examined by microscopy. For time-lapse imaging of Ez-YFP and TD-YFP, transiently transfected 2PK3 cells were adhered in wells of an 8-chambered slide at 5×10^4/ chamber, rinsed with DMEM and stimulated with 10 μg/ml of BLC or DMEM in 100 μl. Recording was started 1 min before stimulation, and resumed for 7 min after addition of BLC or plain medium. Images were collected every 20 s for a period of 8 min. For TIRF microscopy, the focus was adjusted to the interface between the sample and coverslip and laser was aligned to achieve the optimum angle of reflection. All TIRF images were acquired at a depth of 110 nm. All images were acquired using a Leica-AM TIRF microscope DMI6000 (Leica Microsystems) with an attached Hamamatsu EM-CCD camera, using HCX PL APO 100X oil objective with numerical aperture of 1.47 and appropriate filter cubes. The imaging was performed on cells maintained in B cell medium at 37 °C using the Leica acquisition software LAS AF Version 2.2.0.

Image processing

Metamorph image analysis software was used for digital “no-neighbors” 2D deconvolution, pixel intensity and line-scan calculation, and processing of time-lapse movies. Images acquired in the TIRF mode were deconvolved using Metamorph and analyzed further with ImagePro 6.1 using an algorithm specifically written to quantify the number of individual filaments in the contact area and their presence through the duration of imaging. Briefly, a region of interest encompassing the contact area was drawn and extruded into multiple concentric regions of 10-pixel width each. The filaments were “Top Hat” filtered to enhance/equalize their appearance, thresholded, separated from one another (skeletonization, branch-point identification and subtraction), and subsequently counted in each concentric region of interest across the stack of images (acquired every 20 s for 8 min). The total

filament area in each region of interest ring was calculated summing segmented filament pixels (Supplemental Fig. S4). The heat maps were generated to represent the presence of each filament in the different image frames. Briefly, each frame of the segmented filament sequence was divided by 255 such that each positively segmented filament pixel was set to 1. A maximum intensity projection was then generated and pseudo-colored such that a look-up table ranging from blue to red represents filament pixels present in a single image frame (blue) to those persistent in all of the frames (red).

Statistical analyses

Graphs show the mean and standard deviation observed in independent experiments. Exact p values were calculated using the non-parametric two-tailed Mann-Whitney test for the unpaired data sets. Mann-Whitney test is appropriate as the comparison is only between two groups, and each group contains a sample size of ten or more. The tests were performed with 95% confidence interval (alpha level 0.05).

RESULTS

Chemokine stimulation of B cells induces dephosphorylation of ezrin and moesin

We first examined the localization of ERM proteins in resting B cells by imaging endogenous ezrin and moesin in the epifluorescence and TIRF modes. Both proteins were localized in the cortical region beneath the membrane (Fig. 1A, left panels) and enriched in the cell surface microvilli (Fig. 1A, right panels). To examine the effect of chemokine stimulation on the subcellular localization of ezrin, splenic B cells were stimulated with BLC and immunostained for endogenous ezrin and F-actin. In unstimulated resting B cells ezrin was uniformly distributed at the cell cortex, but rapidly relocalized and co-polarized with F-actin upon BLC stimulation (Fig. 1B). The line-scan measurements show an increase in pixel intensity of both ezrin and F-actin at the same position indicating co-polarization (Supplemental Fig. S1A). A similar co-polarization of ezrin with F-actin was observed in the 2PK3 B lymphoma cell line upon BLC treatment (Supplemental Fig. S1B). Since relocalization of ezrin is expected to involve conformational change that depends on phosphorylation at the regulatory T567 site, we measured the phosphorylation of ezrin using a phosphoThrERM-specific antibody. In naïve, mature B cells both ezrin and moesin were constitutively phosphorylated at T567 and T558, respectively (Fig. 1C), consistent with their predominantly cortical localization (Fig. 1A). Stimulation with BLC (Fig. 1C) or SDF-1α (Supplemental Fig. S1C) induced rapid but transient dephosphorylation of ezrin and moesin. Since phosphorylation at the regulatory threonine residue defines the active conformation of ERM proteins, our data indicate that exposure to chemokine induces a conformational switch from the “open” membrane-tethering form to the “closed” dormant form. Chemokine-induced relocalization of ezrin and co-polarization with F-actin was also observed when purified splenic B cells (Supplemental Fig. S2A) or 2PK3 B cells (Supplemental Fig. S2B) were adhered on the physiological substrate fibronectin.

Preventing regulatory threonine dephosphorylation of ERM proteins inhibits B cell migration

To test whether dephosphorylation of the regulatory threonine residues in ezrin and moesin plays a role in B cell migration, we treated B cells with a cell-permeable Ser/Thr phosphatase inhibitor, calyculin A. Treatment of B cells with calyculin A resulted in a dose-dependent inhibition of BLC-induced dephosphorylation of ezrin and moesin (Fig. 2A). We performed dose titration to optimize the concentration of BLC for in vitro migration of B cells and threonine dephosphorylation of the ERM proteins, and chose 1 μg/ml for our experiments (Supplemental Fig. S3). We performed transwell migration assay to examine the effect of preventing dephosphorylation of ezrin and moesin on the ability of B cells to

undergo chemotaxis. Calyculin A treatment inhibited BLC-induced chemotaxis of B cells in a dose-dependent manner (Fig. 2B). Next, we adoptively transferred CD45.2$^+$ C57BL/6 B cells treated with calyculin A into congenic CD45.1$^+$ B6.SJL recipients, and examined their ability to home to the lymph nodes and spleen using an in vivo homing assay. A larger number of calyculin A-treated B cells was found in the blood of the recipient mice (Fig. 2C) than those treated with DMSO at 1.5 h after adoptive transfer. Accordingly, only half of calyculin A-treated B cells were able to home to the recipient spleen at this time (Fig. 2D). A similar defect was also observed in the homing of calyculin A-treated B cells to the lymph nodes and spleen at 26 h post-transfer (Fig. 2E, 2F). These results indicate that ERM dephosphorylation is an important feature of B cell migration. However, incomplete inhibition of B cell homing suggests that additional factors play a role in regulating B cell migration in vivo.

As cell polarization and extension of lamellipodia are early events in cell migration, we examined the effect of Ser/Thr phosphatase inhibition on B cell morphology using high resolution scanning electron microscopy (scanning EM). The resting B cell surface was largely covered with microvilli and very few membrane ruffles (Fig. 2G, top panels). Calyculin A treatment impaired formation of surface microvilli and ruffles in resting B cells (Fig. 2G, bottom panels). Upon stimulation of B cells with BLC, most of the cells showed resorption of microvilli and an increase in the extension of membrane ruffles within 2 min (Fig. 2H; black bars). At 5 min after stimulation, a majority of the cells retained membrane ruffles but started showing a reappearance of microvilli. Most of the stimulated cells reverted back to their original resting morphology within 10 min. The presence of ruffles or microvilli on the B cells was not mutually exclusive and cells that had both ruffles and microvilli were present in the population at all times. However, with increasing duration of stimulation the percentage of cells that showed either ruffles or microvilli changed. Ten percent of the calyculin A-treated cells extended a few stubby projections upon BLC stimulation, but failed to extend membrane ruffles (Fig. 2H; gray bars). These data show that threonine dephosphorylation of ERM proteins is necessary for initiation of morphological changes associated with cell migration.

Expression of a constitutively active form of ezrin inhibits B cell migration

Since calyculin A inhibits Ser/Thr phosphatase activity non-specifically it is likely to prevent other dephosphorylation events within the B cell in addition to dephosphorylation of ERM proteins. To specifically address the requirement for dephosphorylation of ERM proteins on B cell morphology and migration, we utilized a phosphomimetic mutant of ezrin that is trapped in an irreversible constitutively phosphorylated state. In the phosphomimetic mutant of ezrin the regulatory threonine at position 567 was mutated to aspartic acid (T567D) affording constitutive binding to transmembrane proteins and F-actin (24). The plasmid pIRES2-EGFP expressing the active T567D (Supplemental Fig. S4A) mutant of ezrin was transiently transfected into 2PK3 B cells, and bicistronic expression of EGFP was used as a reporter of transfection efficiency (Supplemental Fig. S4B, left). Since the T567D mutant of ezrin is untagged, overexpression of the T567D mutant was assessed by increase in intensity of the protein band corresponding to ezrin in the immunoblot (Supplemental Fig. S4C). Expression of moesin remained unaffected by expression of the T567D mutant of ezrin (Supplemental Fig. S4C). We examined the effect of transiently overexpressing the T567D mutant on B cell migration using an in vitro transwell migration assay. While 93% of the mock-transfected 2PK3 cells migrated in response to BLC, only 61% of GFP$^+$ cells expressing the constitutively active T567D mutant of ezrin were able to migrate (Fig. 3A). CXCR5, the specific receptor for BLC was similarly expressed in mock-transfected and T567D mutant-expressing 2PK3 cells (Supplemental Fig. S4B, right).

Constitutively active ezrin inhibits microvilli formation in resting B cells and prevents BLC-induced membrane ruffling

Next, we tested if 2PK3 cells expressing the T567D mutant are able to change their morphology upon BLC stimulation. Given the heterogeneity of the transiently transfected population, and the inability to distinguish between untransfected and transfected cells by scanning EM, we generated 2PK3 B cell transfectants that stably expressed the T567D mutant of ezrin. We selected stable transfectants of 2PK3 cells exhibiting 100% GFP expression (Supplemental Fig. S4D, left) and CXCR5 expression that was comparable to that of untransfected cells (Supplemental Fig. S4D, right). The T567D-expressing stable transfectants showed 3-fold overexpression of ezrin as compared to the untransfected cells (Supplemental Fig. S4E). Expression of moesin was similar between untransfected 2PK3 cells and those staby expressing the T567D mutant (Supplemental Fig. S4E). Untransfected 2PK3 cells or those stably expressing the T567D mutant were stimulated with BLC and subjected to scanning electron microscopy. Similar to splenic primary B cells, the 2PK3 B cells were rich in surface microvilli (Fig. 3B; top left panel). Within 5 min of BLC-stimulation, a majority of the untransfected 2PK3 cells resorbed their microvilli (Fig. 3B, C, open black bars) and extended membrane ruffles (Fig. 3B, C; filled black bars). In contrast, expression of the constitutively active T567D mutant not only reduced microvilli formation on most of the resting 2PK3 cells making them appear “bald” (Fig. 3B, bottom left panel), but also impaired the induction of membrane ruffles in response to BLC (Fig. 3B; bottom panels). Stimulation of the T567D-expressing cells with BLC induced the appearance of stubby projections in a small fraction of these cells. The quantification of untransfected and T567D-expressing 2PK3 cells bearing microvilli or ruffles or lack thereof is presented in Figure 3C. Together these data demonstrate that restricting membrane-cytoskeletal dynamics by forced expression of the conformationally active mutant of ezrin alters resting B cell morphology and inhibits chemokine-induced polarization, explaining the reduced B cell migration observed in the presence of the T567D mutant of ezrin.

We further examined whether the BLC-dependent signal transduction was affected in the presence of the T567D mutant. Untransfected 2PK3 cells or those stably expressing the T567D mutant of ezrin were stimulated with BLC and cell lysates probed for phosphorylation-dependent activation of signaling proteins in the MAPK and PI3K pathways. Activation of ERK1/2, JNK1/2 and Akt pathways was similarly induced in control and T567D mutant-expressing 2PK3 cells (Supplemental Fig. S5A). These data indicate that the defects observed in migration of B cells expressing the active mutant of ezrin are not a consequence of impaired proximal signaling but result from defect in morphological changes induced by the chemokine. The importance of chemokine-induced PLC activation in initiating the inactivation of ERM proteins is well established in T cells (26). We tested if PLC activation would affect ERM inactivation in B cells and found that inhibition of PLC prevented dephosphorylation of ERM proteins (Supplemental Fig. S5B, S5C). These data indicate that regulation of membrane PIP_2 levels by PLC activity may influence the activation and localization of ERM proteins in B cells as well.

Irreversible tethering of the membrane and actin cytoskeleton inhibits BLC-induced resorption of microvilli

The inability of B cells treated with calyculin A or those expressing the constitutively active mutant of ezrin to form surface microvilli prompted us to closely examine the microvilli dynamics in live B cells stimulated with chemokine. We employed TIRF microscopy to visualize the association of ezrin with microvilli and chemokine-induced changes in ezrin localization on the B cell surface. We transiently expressed YFP fusion proteins of wild type ezrin (Ez-YFP) and the T567D mutant of ezrin (TD-YFP) in 2PK3 cells, and performed time-lapse TIRF imaging to visualize surface dynamics of these proteins in the presence of

BLC. To control for perturbations introduced during addition of BLC, the cells were also imaged upon addition of medium without BLC. In order to quantify individual microvilli dynamics, the contact area in the images were segmented into regions of interest (Supplemental Fig. S6A). The fluorescence intensity of individual microvillar filaments was used to estimate the total filament area in each concentric region of interest. The lifespan of individual filaments following stimulation was determined by plotting filament area in each ROI throughout the time-lapse imaging period as described in Methods. Most 2PK3 cells expressing Ez-YFP revealed a profusion of distinct and spontaneously dynamic microvilli at the site of contact (Fig. 4A, top left, Supplemental video 1). Medium-treated 2PK3 cells expressing Ez-YFP (Fig. 4A, left panels, and Supplemental video 1) or TD-YFP (Fig. 4A, right panels, and Supplemental video 2), showed no variation in total filament area (Fig. 4C', 4D'). Heat mapping of medium-treated 2PK3 cells expressing Ez-YFP (Fig. 4C) showed mostly yellow or red colored filaments indicating that most filaments persisted throughout the duration of imaging. BLC-stimulation of cells expressing Ez-YFP induced resorption of microvilli with time (Fig. 4B, left panels, and Supplemental video 3), as reflected in the mostly blue and cyan-colored filaments in the heat map (Fig. 4E), and reduced total filament area following stimulation (Fig. 4E'). 2PK3 cells expressing TD-YFP showed a greatly reduced number of microvilli at the site of contact, (Fig. 4A, B, top right panels) and an almost flat "bald" surface, consistent with our previous scanning EM data (Fig. 3B). Stimulation of TD-YFP-expressing 2PK3 cells with BLC (Fig. 4B, right panels, and Supplemental video 4) resulted in no change in the lifespan of the minimal surface projections that were mostly green in color (Fig. 4F). TD-YFP-expressing 2PK3 cells showed a slight increase in the total filament area (Fig. 4F') in response to BLC treatment that may be due to the appearance of stubby protrusions, similar to those observed with scanning EM imaging (Fig. 3B, bottom panels). Our live TIRF imaging data together with the high magnification scanning EM images reveal that dynamic local changes in the conformation of ezrin are necessary for the formation and maintenance of microvilli on the B cell surface. Further, resorption of microvilli is an early event in BLC-induced cell polarization and migration that involves conformational inactivation of ezrin.

BLC-induced relocation of constitutively active ezrin is impaired

Polarization of endogenous ezrin and F-actin in response to BLC suggested a potential role for ezrin at the front pole of migrating B cells. To compare chemokine-induced partitioning of wild type and T567D mutant of ezrin in live cells, we performed time-lapse epifluorescence imaging of Ez-YFP and TD-YFP in 2PK3 cells. Similar to endogenous ezrin, the Ez-YFP fusion protein was localized predominantly in the cortical region of the cell (Fig. 5A), but underwent relocation to the lamellipodia following BLC-stimulation (Fig. 5A, D, and Supplemental video 5). 2PK3 B cells expressing TD-YFP showed two distinct patterns of localization, with 40% of cells showing uniform cortical distribution (Fig. 5B) and 60% of cells showing pre-polarized localization (Fig. 5C). Constitutively polarized TD-YFP was enriched at what appeared to be the contact point between the cells and the substratum. Therefore, we examined the localization of adhesion molecules such as CD44 that accumulate at sites of contact with the substratum. TD-YFP co-localized with CD44 (Supplemental Fig. 6B, C) regardless of the presence or absence of BLC. 2PK3 cells with uniform distribution of CD44 showed a similar uniform distribution of TD-YFP, and cells with polarized CD44 showed co-polarization of TD-YFP. These results indicate that contact-induced polarization of adhesion proteins such as CD44 forces the constitutively active T567D mutant of ezrin to assume a polarized distribution at the site of strongest adhesion. Regardless of the initial localization TD-YFP failed to redistribute to the leading edge in response to BLC stimulation (Fig. 5B, C, D and Supplemental videos 6, 7). Our results indicate that the mobility and partitioning of the constitutively active mutant of ezrin is compromised.

Constitutively active ezrin is unable to co-polarize with F-actin in response to BLC

Next, we examined whether BLC-induced polarization of Ez-YFP coincides with that of F-actin. In resting 2PK3 cells, Ez-YFP was uniformly co-distributed with F-actin (Fig. 6A), as observed earlier with endogenous ezrin (Fig. 1B). Upon stimulation with BLC, Ez-YFP co-polarized with F-actin (Fig. 6A, bottom three rows, and Fig. 6C). The line-scan measurements show an increase in pixel intensity of both ezrin and F-actin at the same position indicating co-polarization (Supplemental Fig. S6D). In contrast, TD-YFP failed to co-polarize with F-actin (Fig. 6B, bottom three rows, and Fig. 6C) indicating a marked defect in the partitioning of ezrin. The line-scan measurements show an increase in pixel intensity only of F-actin and not ezrin indicating absence of co-localization (Supplemental Fig. S6E). These data show that expression of TD-YFP did not affect the ability of cells to polymerize F-actin in response to BLC stimulation. Instead, the mobility of the T567D mutant in response to chemokine was grossly inhibited.

DISCUSSION

We have used a combination of scanning EM, epiflourescence and TIRF microscopy to perform a systematic visual analysis of the earliest changes occurring in chemokine-stimulated B cells. Our data provide evidence that dynamic changes in the conformation of ezrin regulate B cell morphology and migration. We show that chemokine-induced dephosphorylation of the regulatory threonine in ezrin regulates its polarization to the F-actin-rich front pole of migrating B cells. TIRF imaging of both live and fixed B cells showed an abundance of surface microvilli rich in ezrin and moesin. A proteomic analysis of microvilli was reported to show a similar enrichment of the ERM proteins, ezrin and moesin in these membrane structures isolated from human T cells (30). As reported by others, we also observed chemokine-induced threonine dephosphorylation of both ezrin and moesin in B cells supporting the notion that these proteins function in a redundant manner to facilitate chemotaxis (31, 32). We have employed TIRF microscopy to image microvilli resorption in live B cells stimulated with chemokines. Inhibition of Ser/Thr phosphatase activity in B cells with calyculin A resulted in an impairment in the generation of surface microvilli altogether, suggesting that local and rapid changes in ERM conformation are necessary for the maintenance and dynamic behavior of microvilli. Calyculin A treatment also caused a loss of chemokine-dependent membrane ruffling and a marked reduction in B cell chemotaxis. Dephosphorylation of ERM proteins appears to be required for their detachment from the microvillar membrane and the supporting F-actin filaments in order to initiate resorption of the microvilli and extension of membrane ruffles. Inhibition of phosphatase activity in neutrophils was similarly reported to result in impaired neutrophil migration. Dephosphorylation of the regulatory T558 residue in moesin was suggested as a necessary step for release and retraction of the uropod during neutrophil migration (33). Inactivation of ERM proteins in chemokine-stimulated T cells is initiated by the reduction of membrane PIP_2 levels upon activation of PLC (26). Our results show that inhibition of PLC prevents chemokine-induced ERM dephosphorylation in B cells indicating that PLC activity may similarly regulate PIP_2 levels in B cells to initiate chemotaxis.

Expression of the constitutively active mutant of ezrin also resulted in “bald” B cells with no surface microvilli, consistent with the effect of Ser/Thr phosphatase inhibition on B cell morphology. In contrast to untransfected 2PK3 B cells, even at ten minutes after chemokine-stimulation, 2PK3 cells expressing the T567D mutant of ezrin failed to induce membrane ruffles. A similar dependence of chemokine-induced microvilli resorption on ERM dephosphorylation was reported in human peripheral blood T cells (31). Our results show that the constitutively active mutant of ezrin acts in a dominant negative manner to restrict spontaneous microvilli formation and prevents chemokine-induced membrane ruffling. Restricted dynamics of these actin-rich membranous structures is likely contribute towards

reduced B cell migration observed in the presence of the constitutively active mutant of ezrin. The expression of the T567D mutant of ezrin only caused a partial inhibition of B cell migration, suggesting that ERM dephosphorylation is one of many factors contributing to the regulation of B cell migration. In our study, the constitutively active mutant of ezrin was found to spontaneously polarize in a majority of the 2PK3 B cells, while it was uniformly distributed in the remaining cells. Live imaging of BLC-stimulated 2PK3 B cells revealed that irrespective of its localization, the constitutively active mutant of ezrin was unable to relocalize to the leading edge with F-actin. Our results show that polarization of adhesion molecules such as CD44, induced upon strong attachment to the substratum, can force polarization of the constitutively active mutant of ezrin. CD44 was reported to regulate adhesion and polarize to the uropod in chemokine-stimulated T cells (20, 34, 35). Our results suggest that the constitutively active nature of the phosphomimetic mutant of ezrin forces its irreversible association with CD44, and may block uropod detachment and retraction.

Signaling initiated by chemokine receptor engagement regulates cell adhesion and F-actin polymerization. In B cells, chemokine receptor mediated activation of PI3K was reported to regulate B cell adhesion and migration (36). The expression of constitutively active ezrin in 2PK3 cells did not affect BLC-dependent activation of MAPK and PI3K activation. Actin polymerization also remained unaffected in B cells expressing the active mutant of ezrin indicating that dephosphorylation of ezrin is not required for the pathway leading to the nucleation of new actin filaments. Instead, ezrin dephosphorylation primarily acts by facilitating membrane-cytoskeletal tethering and untethering. Stimulation of mouse splenic B cells and 2PK3 B cells with BLC resulted in redistribution of ezrin at the F-actin-rich front edge. Our data indicate that transient dephosphorylation of ezrin mediates its relocation, however, the exact mechanism of relocation is unclear. LOK was recently shown to phosphorylate ERM proteins in human peripheral blood lymphocytes as well as those in murine peripheral lymphoid organs (25). Interestingly, lymphocytes from mice lacking LOK show enhanced F-actin polarization in response to chemokine stimulation, suggesting that this kinase plays an important role in regulating the equilibrium between phosphorylated and unphosphorylated ERM proteins, contributing to their localization during initiation of lymphocyte migration. In breast carcinoma cells conformationally active ezrin recruited Cdc42/Rho-specific guanine nucleotide exchange factor Dbl to the GM1-containing lipid raft microdomains (37). This recruitment was proposed as a mechanism of activation of Cdc42 at the lamellipodia facilitating morphological changes and directed cell migration (37). In gastric parietal cells the rapid turnover of T567 phosphorylated ezrin in the steady state is known to keep membrane activity in a dynamic state (38). We suggest that the redistribution of ezrin to the front of migrating B cells may serve to orchestrate rapidly evolving membrane-actin contacts at the lamellipodia. Since constitutively active T567D ezrin is already tightly associated with the membrane and cortical actin, it fails to dissociate and re-associate with the freshly polymerized and polarized F-actin at the front end and participate in lamellipodial protrusion.

Ezrin is the only ERM family protein expressed in polarized epithelial cells of the small intestine (39, 40) whose surface is covered with dense brush border microvilli. Deficiency of ezrin in mice results in abnormal villus morphogenesis and neonatal death (41). Ezrin was shown to be critical for organizing the apical domain of the intestinal epithelial cells and its associated apical junctions (41). Further, ultra-thin section EM analysis of gastric parietal cells in mice shows a secretory canaliculus structure, which is composed of invaginations of the apical surface bearing numerous microvilli that interact with the tubulovesicular structures that underlie the apical canaliculi. In ezrin knockdown mice the parietal cells lack invaginated apical canaliculi that do not expand even in the presence of histamine (42). Our data are in agreement with these studies wherein ezrin localization was shown to be

important for appropriate membrane contacts. Since the membrane localization of ezrin and its ability to link with actin filaments are regulated by phosphorylation of its regulatory T567 site, rapid and transient changes in phosphorylation of ezrin may orchestrate the dynamic membrane-actin contacts at the lamellipodial front.

An in-depth visual analysis of B cells using high-resolution and live cell imaging revealed a requirement of dephosphorylation of ERM proteins in B cell chemotaxis. Our data indicate that local changes in ezrin conformation are critical for the generation and maintenance of microvilli in resting B cells and their conversion to dynamic lamellipodia in the presence of a chemokine. The relocation of ezrin to the lamellipodia suggests a role for it in facilitating spatiotemporal molecular partitioning, and/or in maintaining the dynamic nature of the front end of the migrating B cells.

Supplementary Material

Refer to Web version on PubMed Central for supplementary material.

Acknowledgments

The authors would like to thank Twishasri Dasgupta for help with construction of the YFP fusion proteins used in this study, Jennifer Powers for cell sorting, the Lerner Research Institute Imaging core personnel for help with imaging and Dr. Amit Vasanji of the Biomedical Imaging and Analysis core for help with analysis of the TIRF data.

This work was supported by grants from the National Institute for Allergy and Infectious Diseases (AI081743), National Institute of Diabetes, Digestive and Kidney Diseases (DK068242) and an Investigator Award from the Cancer Research Institute to N.G.

References

1. Cyster JG. Chemokines, sphingosine-1-phosphate, and cell migration in secondary lymphoid organs. Annu Rev Immunol. 2005; 23:127–159. [PubMed: 15771568]
2. Wang A, Fairhurst AM, Tus K, Subramanian S, Liu Y, Lin F, Igarashi P, Zhou XJ, Batteux F, Wong D, Wakeland EK, Mohan C. CXCR4/CXCL12 hyperexpression plays a pivotal role in the pathogenesis of lupus. J Immunol. 2009; 182:4448–4458. [PubMed: 19299746]
3. Nanki T, Takada K, Komano Y, Morio T, Kanegane H, Nakajima A, Lipsky PE, Miyasaka N. Chemokine receptor expression and functional effects of chemokines on B cells: implication in the pathogenesis of rheumatoid arthritis. Arthritis Res Ther. 2009; 11:R149. [PubMed: 19804625]
4. Burkle A, Niedermeier M, Schmitt-Graff A, Wierda WG, Keating MJ, Burger JA. Overexpression of the CXCR5 chemokine receptor, and its ligand, CXCL13 in B-cell chronic lymphocytic leukemia. Blood. 2007; 110:3316–3325. [PubMed: 17652619]
5. Kurtova AV, Tamayo AT, Ford RJ, Burger JA. Mantle cell lymphoma cells express high levels of CXCR4, CXCR5, and VLA-4 (CD49d): importance for interactions with the stromal microenvironment and specific targeting. Blood. 2009; 113:4604–4613. [PubMed: 19228923]
6. Ehlin-Henriksson B, Liang W, Cagigi A, Mowafi F, Klein G, Nilsson A. Changes in chemokines and chemokine receptor expression on tonsillar B cells upon Epstein-Barr virus infection. Immunology. 2009; 127:549–557. [PubMed: 19604305]
7. Bromley SK, Mempel TR, Luster AD. Orchestrating the orchestrators: chemokines in control of T cell traffic. Nat Immunol. 2008; 9:970–980. [PubMed: 18711434]
8. Okada T, Miller MJ, Parker I, Krummel MF, Neighbors M, Hartley SB, O'Garra A, Cahalan MD, Cyster JG. Antigen-engaged B cells undergo chemotaxis toward the T zone and form motile conjugates with helper T cells. PLoS Biol. 2005; 3:e150. [PubMed: 15857154]
9. Rafelski SM, Theriot JA. Crawling toward a unified model of cell mobility: spatial and temporal regulation of actin dynamics. Annu Rev Biochem. 2004; 73:209–239. [PubMed: 15189141]

10. Vicente-Manzanares M, Sanchez-Madrid F. Role of the cytoskeleton during leukocyte responses. Nat Rev Immunol. 2004; 4:110–122. [PubMed: 15040584]
11. Fukui Y, Hashimoto O, Sanui T, Oono T, Koga H, Abe M, Inayoshi A, Noda M, Oike M, Shirai T, Sasazuki T. Haematopoietic cell-specific CDM family protein DOCK2 is essential for lymphocyte migration. Nature. 2001; 412:826–831. [PubMed: 11518968]
12. Pearce G, Angeli V, Randolph GJ, Junt T, von Andrian U, Schnittler HJ, Jessberger R. Signaling protein SWAP-70 is required for efficient B cell homing to lymphoid organs. Nat Immunol. 2006; 7:827–834. [PubMed: 16845395]
13. McLeod SJ, Li AH, Lee RL, Burgess AE, Gold MR. The Rap GTPases regulate B cell migration toward the chemokine stromal cell-derived factor-1 (CXCL12): potential role for Rap2 in promoting B cell migration. J Immunol. 2002; 169:1365–1371. [PubMed: 12133960]
14. McLeod SJ, Shum AJ, Lee RL, Takei F, Gold MR. The Rap GTPases regulate integrin-mediated adhesion, cell spreading, actin polymerization, and Pyk2 tyrosine phosphorylation in B lymphocytes. J Biol Chem. 2004; 279:12009–12019. [PubMed: 14701796]
15. Durand CA, Westendorf J, Tse KW, Gold MR. The Rap GTPases mediate CXCL13- and sphingosine1-phosphate-induced chemotaxis, adhesion, and Pyk2 tyrosine phosphorylation in B lymphocytes. Eur J Immunol. 2006; 36:2235–2249. [PubMed: 16821235]
16. Chen Y, Yu M, Podd A, Wen R, Chrzanowska-Wodnicka M, White GC, Wang D. A critical role of Rap1b in B-cell trafficking and marginal zone B-cell development. Blood. 2008; 111:4627–4636. [PubMed: 18319399]
17. de Gorter DJ, Beuling EA, Kersseboom R, Middendorp S, van Gils JM, Hendriks RW, Pals ST, Spaargaren M. Bruton's tyrosine kinase and phospholipase Cgamma2 mediate chemokine-controlled B cell migration and homing. Immunity. 2007; 26:93–104. [PubMed: 17239630]
18. Rickert P, Weiner OD, Wang F, Bourne HR, Servant G. Leukocytes navigate by compass: roles of PI3Kgamma and its lipid products. Trends Cell Biol. 2000; 10:466–473. [PubMed: 11050418]
19. Weiner OD. Regulation of cell polarity during eukaryotic chemotaxis: the chemotactic compass. Curr Opin Cell Biol. 2002; 14:196–202. [PubMed: 11891119]
20. Sanchez-Madrid F, del Pozo MA. Leukocyte polarization in cell migration and immune interactions. EMBO J. 1999; 18:501–511. [PubMed: 9927410]
21. Kehrl JH. Chemoattractant receptor signaling and the control of lymphocyte migration. Immunol Res. 2006; 34:211–227. [PubMed: 16891672]
22. Bretscher A, Edwards K, Fehon RG. ERM proteins and merlin: integrators at the cell cortex. Nat Rev Mol Cell Biol. 2002; 3:586–599. [PubMed: 12154370]
23. Fievet B, Louvard D, Arpin M. ERM proteins in epithelial cell organization and functions. Biochim Biophys Acta. 2007; 1773:653–660. [PubMed: 16904765]
24. Fievet BT, Gautreau A, Roy C, Del Maestro L, Mangeat P, Louvard D, Arpin M. Phosphoinositide binding and phosphorylation act sequentially in the activation mechanism of ezrin. J Cell Biol. 2004; 164:653–659. [PubMed: 14993232]
25. Belkina NV, Liu Y, Hao JJ, Karasuyama H, Shaw S. LOK is a major ERM kinase in resting lymphocytes and regulates cytoskeletal rearrangement through ERM phosphorylation. Proc Natl Acad Sci U S A. 2009; 106:4707–4712. [PubMed: 19255442]
26. Hao JJ, Liu Y, Kruhlak M, Debell KE, Rellahan BL, Shaw S. Phospholipase C-mediated hydrolysis of PIP2 releases ERM proteins from lymphocyte membrane. J Cell Biol. 2009; 184:451–462. [PubMed: 19204146]
27. Gupta N, Wollscheid B, Watts JD, Scheer B, Aebersold R, DeFranco AL. Quantitative proteomic analysis of B cell lipid rafts reveals that ezrin regulates antigen receptor-mediated lipid raft dynamics. Nat Immunol. 2006; 7:625–633. [PubMed: 16648854]
28. Bruce B, Khanna G, Ren L, Landberg G, Jirstrom K, Powell C, Borczuk A, Keller ET, Wojno KJ, Meltzer P, Baird K, McClatchey A, Bretscher A, Hewitt SM, Khanna C. Expression of the cytoskeleton linker protein ezrin in human cancers. Clin Exp Metastasis. 2007; 24:69–78. [PubMed: 17370041]
29. Reif K, Cyster JG. RGS molecule expression in murine B lymphocytes and ability to down-regulate chemotaxis to lymphoid chemokines. J Immunol. 2000; 164:4720–4729. [PubMed: 10779778]

30. Hao JJ, Wang G, Pisitkun T, Patino-Lopez G, Nagashima K, Knepper MA, Shen RF, Shaw S. Enrichment of distinct microfilament-associated and GTP-binding-proteins in membrane/microvilli fractions from lymphoid cells. J Proteome Res. 2008; 7:2911–2927. [PubMed: 18505283]

31. Brown MJ, Nijhara R, Hallam JA, Gignac M, Yamada KM, Erlandsen SL, Delon J, Kruhlak M, Shaw S. Chemokine stimulation of human peripheral blood T lymphocytes induces rapid dephosphorylation of ERM proteins, which facilitates loss of microvilli and polarization. Blood. 2003; 102:3890–3899. [PubMed: 12907449]

32. Nijhara R, van Hennik PB, Gignac ML, Kruhlak MJ, Hordijk PL, Delon J, Shaw S. Rac1 mediates collapse of microvilli on chemokine-activated T lymphocytes. J Immunol. 2004; 173:4985–4993. [PubMed: 15470041]

33. Yoshinaga-Ohara N, Takahashi A, Uchiyama T, Sasada M. Spatiotemporal regulation of moesin phosphorylation and rear release by Rho and serine/threonine phosphatase during neutrophil migration. Exp Cell Res. 2002; 278:112–122. [PubMed: 12126963]

34. Gerard A, Mertens AE, van der Kammen RA, Collard JG. The Par polarity complex regulates Rap1- and chemokine-induced T cell polarization. J Cell Biol. 2007; 176:863–875. [PubMed: 17353362]

35. Barreiro O, de la Fuente H, Mittelbrunn M, Sanchez-Madrid F. Functional insights on the polarized redistribution of leukocyte integrins and their ligands during leukocyte migration and immune interactions. Immunol Rev. 2007; 218:147–164. [PubMed: 17624951]

36. Ortolano S, Hwang YI, Han SB, Kehrl JH. Roles for phosphoinositide 3-kinases, Bruton's tyrosine kinase, and Jun kinases in B lymphocyte chemotaxis and homing. Eur J Immunol. 2006; 36:1285–1295. [PubMed: 16619289]

37. Prag S, Parsons M, Keppler MD, Ameer-Beg SM, Barber P, Hunt J, Beavil AJ, Calvert R, Arpin M, Vojnovic B, Ng T. Activated ezrin promotes cell migration through recruitment of the GEF Dbl to lipid rafts and preferential downstream activation of Cdc42. Mol Biol Cell. 2007; 18:2935–2948. [PubMed: 17538024]

38. Zhu L, Zhou R, Mettler S, Wu T, Abbas A, Delaney J, Forte JG. High turnover of ezrin T567 phosphorylation: conformation, activity, and cellular function. Am J Physiol Cell Physiol. 2007; 293:C874–884. [PubMed: 17553936]

39. Berryman M, Franck Z, Bretscher A. Ezrin is concentrated in the apical microvilli of a wide variety of epithelial cells whereas moesin is found primarily in endothelial cells. J Cell Sci. 1993; 105(Pt 4):1025–1043. [PubMed: 8227193]

40. Ingraffea J, Reczek D, Bretscher A. Distinct cell type-specific expression of scaffolding proteins EBP50 and E3KARP: EBP50 is generally expressed with ezrin in specific epithelia, whereas E3KARP is not. Eur J Cell Biol. 2002; 81:61–68. [PubMed: 11893083]

41. Saotome I, Curto M, McClatchey AI. Ezrin is essential for epithelial organization and villus morphogenesis in the developing intestine. Dev Cell. 2004; 6:855–864. [PubMed: 15177033]

42. Tamura A, Kikuchi S, Hata M, Katsuno T, Matsui T, Hayashi H, Suzuki Y, Noda T, Tsukita S. Achlorhydria by ezrin knockdown: defects in the formation/expansion of apical canaliculi in gastric parietal cells. J Cell Biol. 2005; 169:21–28. [PubMed: 15809309]

ABBREVIATIONS

BLC	B lymphocyte chemokine
ERM	ezrin-radixin-moesin
SDF-1α	Stromal cell derived factor-1α
PIP_2	Phosphatidylinositol bisphosphate
PLC	Phospholipase C
TIRF	total internal reflection fluorescence

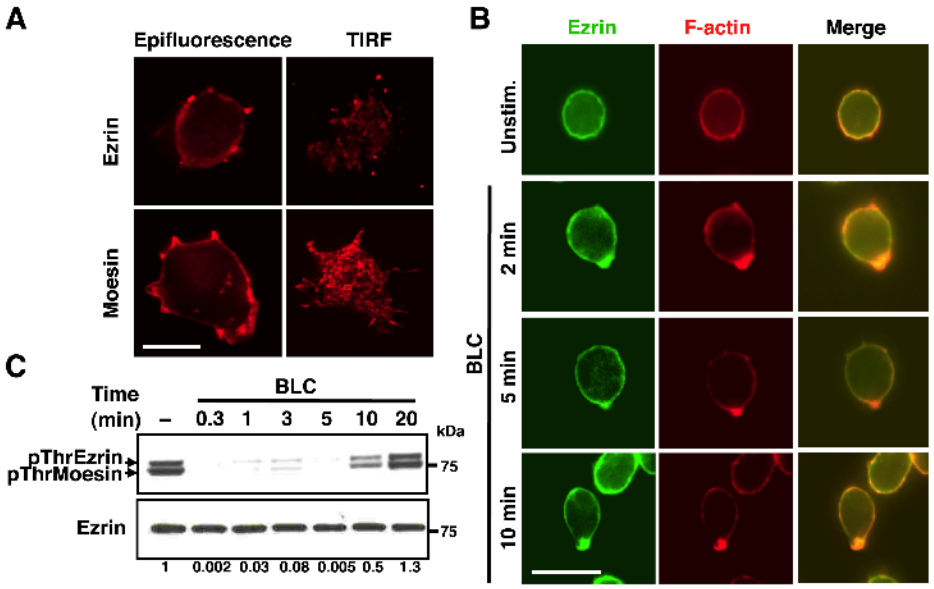

Figure 1. BLC stimulation induces co-polarization of ezrin with actin and dephosphorylation of ezrin at T567

(A) 2PK3 cells were stained for ezrin and moesin, and imaged in the epifluorescence or TIRF mode at an additional 1.6x magnification with a 100x objective. Scale bar, 5 μm. **(B)** Purified splenic B cells were stimulated with 10 μg/ml BLC for the indicated times and fixed prior to staining for ezrin and F-actin. Scale bar, 5 μm. **(C)** Splenic B cells were stimulated with 3 μg/ml of BLC for indicated lengths of time and lysates were probed with pThrERM or ezrin antibody. The numbers shown below are ratio of pThrERM to total ezrin calculated from densitometric analysis of the immunoblots. Data are representative of two independent experiments.

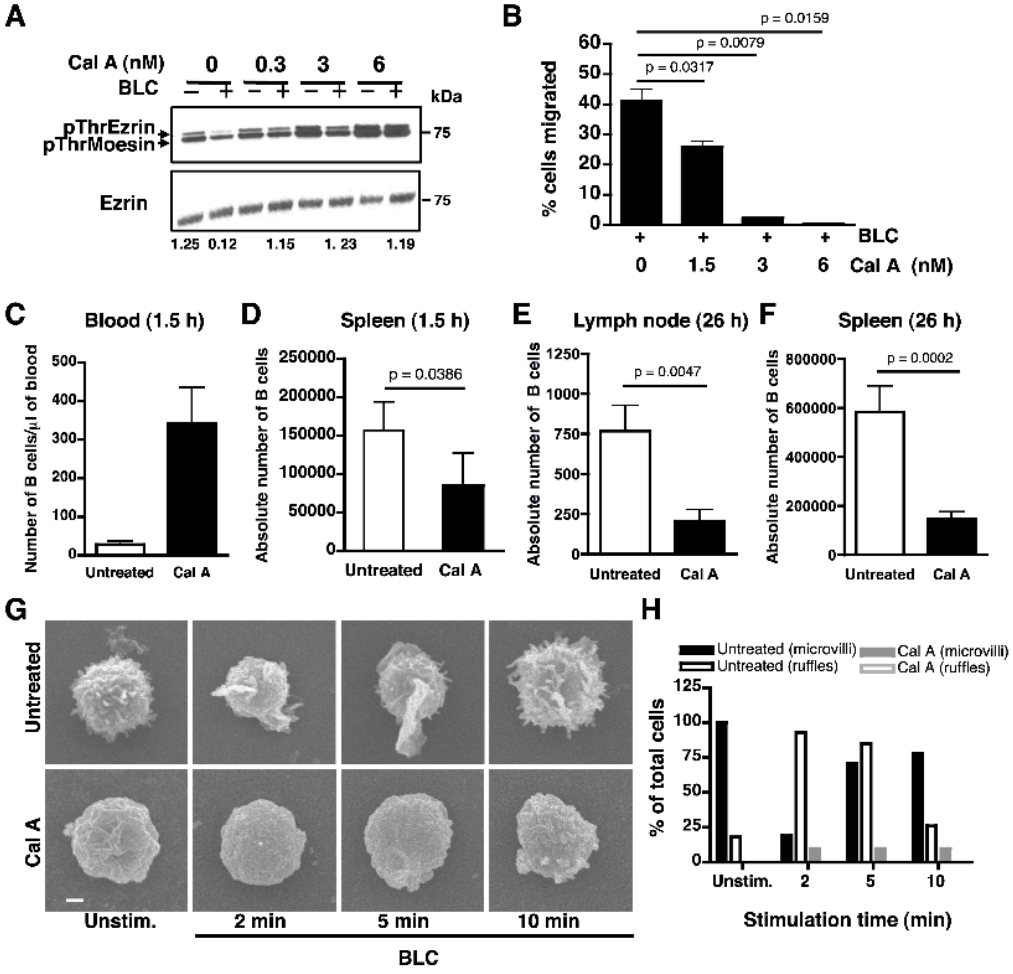

Figure 2. Inhibition of Ser/Thr phosphatase activity impairs B cell migration

(A) Splenic B cells were pretreated with the indicated doses of calyculin A, left unstimulated or stimulated with 1 μg/ml of BLC for 1 min and lysates were probed with pThrERM or ezrin antibody. Ratio of pThr ezrin to total ezrin in the stimulated samples was calculated from densitometric analysis of the immunoblot. Data are representative of three independent experiments. **(B)** B cells were pretreated with indicated doses of calyculin A, and subjected to transwell migration in response to 1 μg/ml of BLC. Data are average of three independent experiments (mean±SD). **(C-D)** In vivo homing of purified CD45.2$^+$ B cells from B6 mice either pre-treated with calyculin A (filled bar) or not (empty bar) to spleen of CD45.1$^+$ BoyJ recipients. Bar graph represents number of donor B cells in one microliter of recipient blood **(C)** and absolute numbers of donor B cells in the recipient spleen **(D)** at 1.5 h post-transfer. Data in (D) are an average of four independent experiments (n=5 per experiment, mean ±SD). **(E-F)** Bar graphs represent the absolute number of donor B cells in the recipient lymph nodes **(E)** and spleen **(F)** at 26 h post-transfer. Data are an average of two independent experiments (n=5 per experiment, mean±SD). **(D)** Scanning EM analysis of purified B cells from B6 mice that were left untreated or treated with 6 nM calyculin A followed by stimulation with BLC. Scale bar, 1 μm. **(E)** Percentage of cells (n=20) from untreated (black bars) or calyculin A-treated (gray bars) B cells, that showed presence of microvilli (filled bars) or membrane ruffles (empty bars) on their surface.

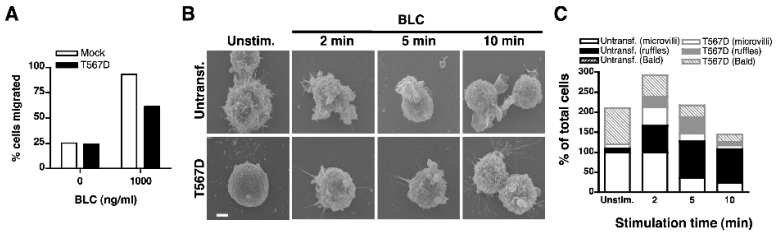

Figure 3. Expression of constitutively active ezrin in B cells decreases in vitro B cell migration, blocks surface microvilli formation and BLC-induced membrane ruffling

(A) Transwell migration of 2PK3 cells that were mock transfected (empty bars) or transfected with the T567D mutant of ezrin (filled bars) in response to 1 μg/ml of BLC. The bar graph shows percent migration for GFP^+ cells. **(B)** Scanning EM images of untransfected 2PK3 cells or those stably expressing the T567D mutant, that were left unstimulated or stimulated with 10 μg/ml of BLC for the indicated times. Scale bar, 1 μm. **(C)** Quantification of untransfected 2PK3 cells (black bars) or those expressing the T567D mutant (gray bars), that showed presence of microvilli (empty bars) or membrane ruffles (filled bars) on their surface or were devoid of both microvilli and ruffles and hence identified as “bald” (patterned bars). Data are shown as a percent of total cells (n=20) analyzed and are representative of two independent experiments.

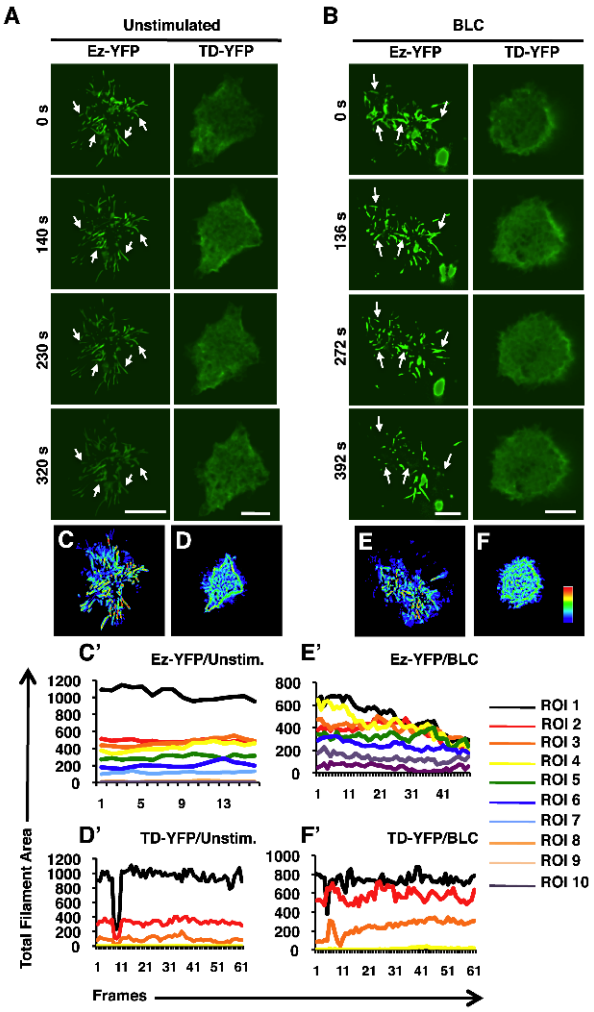

Figure 4. Constitutively active ezrin inhibits BLC-induced resorption of microvilli

TIRF imaging was performed on 2PK3 cells transiently transfected with Ez-YFP or TD-YFP that were left unstimulated **(A, C, D)** or stimulated with 10 μg/ml of BLC **(B, E, F)** in a live time-lapse mode for 8 min. Serial still images are shown for the indicated times of the time-lapse movies. Images were acquired every 20 s with a 100x objective. Scale bar, 5 μm. Arrows mark the positions of microvilli throughout the duration of imaging. Heat maps generated from images of unstimulated **(C, D)** and stimulated **(E, F)** 2PK3 cells expressing Ez-YFP **(C, E)** and TD-YFP **(D, F)**, represent the presence of individual filaments at the surface during the 8 min stimulation period. Coloring scheme represents the filaments that were present in a single frame (blue) versus those present in all the frames (red). The line graphs generated from images of unstimulated **(C', D')** and stimulated **(E', F')** 2PK3 cells expressing Ez-YFP **(C', E')** and TD-YFP **(D', F')**, represent the total filament area in each ROI throughout the different image frames. The ROIs are numbered with one representing the innermost region (Supplemental Fig. S6A). The ROI analysis was performed for multiple cells (n=10), however the ROIs (Supplemental Fig. S6A), heat maps (Fig. 4C-F) and the line graphs (Fig. 4C'-F') are the analysis shown for the representative cells presented in Fig. 4A and 4B.

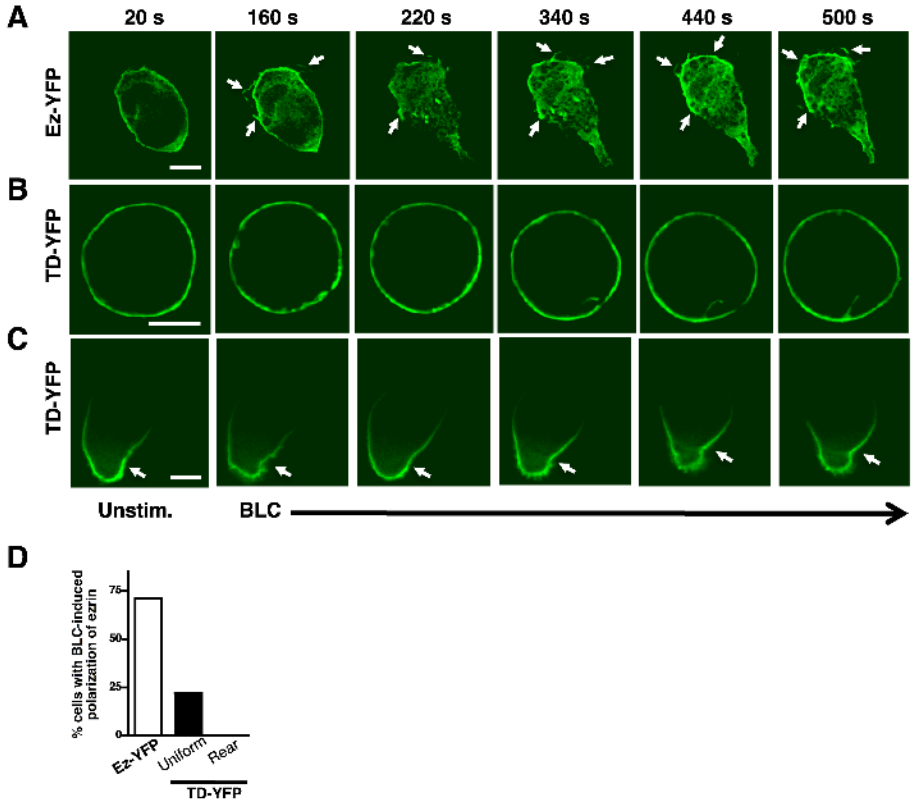

Figure 5. Constitutively active ezrin is unable to polarize in response to BLC

2PK3 cells expressing Ez-YFP **(A)** or TD-YFP **(B, C)** distributed uniformly **(B)** or polarized at the rear end **(C)** were stimulated with 10 μg/ml of BLC and images were acquired every 20 s. Still images are shown for cells at the indicated times during the time-lapse imaging (n=15 per group). Scale bar, 5 μm. Arrows mark concentration of ezrin in membrane ruffles at the front of the polarized cell. **(D)** Quantification of cells in **(A, B, C)** that show BLC-induced polarization of ezrin, as a percentage of total cells (n=15).

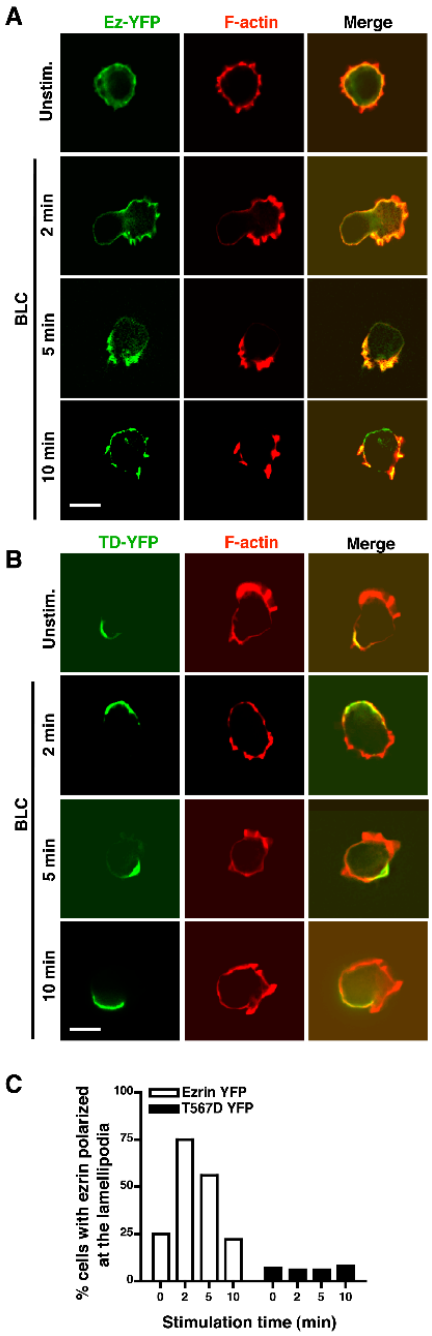

Figure 6. Constitutively active ezrin is unable to co-polarize with F-actin in response to BLC

2PK3 cells were transiently transfected with Ez-YFP **(A)** or TD-YFP **(B)**, stimulated with 10 μg/ml BLC for the indicated times, stained for F-actin and imaged in the epifluorescence mode. Scale bar, 5 μm. **(C)** B cells from (A) and (B) showing co-polarization of ezrin with F-actin are shown as a percentage of the total cells. Data are representative of two independent experiments (n=20 per group).